Notes on the terminal region enlargement of a stabilizing NMPC design for a multicopter

Huu Thien Nguyen, Ngoc Thinh Nguyen, Ionela Prodan

Automatica 159 (2024) 111375

Contents lists available at ScienceDirect

Automatica

journal homepage: www.elsevier.com/locate/automatica

Brief paper

Notes on the terminal region enlargement of a stabilizing NMPC design for a multicopter☆

Huu Thien Nguyen [a,*], Ngoc Thinh Nguyen [b], Ionela Prodan [c]

[a] SYSTEC–ARISE, University of Porto, Porto, Portugal
[b] University of Luebeck, Institute for Robotics and Cognitive Systems, Luebeck, Germany
[c] Université Grenoble Alpes, Grenoble INP[1], LCIS, F-26000, Valence, France

ARTICLE INFO

Article history:
Received 19 December 2022
Received in revised form 4 September 2023
Accepted 26 September 2023
Available online 31 October 2023

Keywords:
Multicopters
NMPC (Nonlinear Model Predictive Control)
Terminal invariant set
Semi-globally asymptotic stability

ABSTRACT

This work proposes an NMPC scheme for stabilizing multicopter dynamics with semi-globally asymptotic stability guarantees. Recurrent issues in the state of the art, such as the existence of a terminal invariant set and a decreasing terminal cost under a local controller are analyzed. Within this context, the novelty resides in the use of a nonlinear local controller with feedback linearization properties which allows for arbitrary enlargement of the ellipsoidal terminal region with respect to the initial conditions. The framework is completed through a detailed analysis of the NMPC parameters. Comparisons and simulations for a nanodrone system show the benefits of the approach.

1. Introduction

Popular multicopter platforms come with built-in controllers which control the rotors to track the four inputs consisting of the thrust level and the three Euler angles (Nascimento & Saska, 2019). Hence, controlling the multicopters reduces to the control of their translational dynamics (Nguyen et al., 2020). However, designing such a high-level controller is difficult due to the complex mix of nonlinear dynamics and constraints of the drones. For control problems with constraints, MPC is a widely embraced technique due to its capability of providing optimal solutions while handling constraints (Alamir, 2018), meanwhile, the closed-loop asymptotic stability is guaranteed by the existence of a positively invariant terminal set and a Lyapunov function associated to the terminal cost (Mayne et al., 2000).

In this work, we focus on an NMPC design with semi-global stability guarantees (Braslavsky & Middleton, 1996) obtained via an appropriate enlargement of the terminal constraint set for a multicopter. The proposed design uses a terminal invariant set with an associated feedback linearization (FL) local controller (Nguyen et al., 2021), which can guarantee the solution existence and closed-loop asymptotic stability only after the first successful iteration (cf. recursive feasibility). With a terminal constraint, the system must initially start close to the terminal region since the predicted state at the end of the prediction horizon must be inside the terminal set. A solution is to increase the prediction horizon but with an unavoidable cost of computation, which could even be impractical in real multicopter systems. Here, we increase instead the size of the terminal set. Note that, tuning the set is difficult due to the complexity of the existing NMPC designs with guaranteed stability, because the tuning parameters do not directly or easily parameterize the terminal set and the resulting attractive region. Consequently, the procedures are often heuristic (repeated tuning/checking iterations) or conservative (due to assumptions which are restrictive) (Cannon et al., 2003; Magni & Scattolini, 2004). One popular approach is the *quasi-infinite horizon* NMPC (qsMPC) design (Chen & Allgöwer, 1998) where the size of the terminal constraint set has to be scaled to ensure the admissible properties and the stability, hence, any modifications on the tuning parameters demand additional re-checks.

Several authors have been working on terminal set enlargement approaches. De Doná et al. (2002) modify the terminal set and the terminal cost based on a saturated linear feedback controller, which serves as a local controller. Cannon et al. (2004) use the concept of partial invariant sets and solve offline linear programming problems to maximize the volume of partially invariant polytopic sets. Limon et al. (2005) compute the sequence of reachable sets using the inner-approximations of one-step sets to construct a contractive terminal set. Brunner et al. (2013) compute the terminal set as a convex hull of the translated and scaled invariant sets along the predicted trajectory.

☆ The material in this paper was not presented at any conference. This paper was recommended for publication in revised form by Associate Editor Prashant Mhaskar under the direction of Editor Thomas Parisini.

* Correspondence to: Faculty of Engineering, University of Porto, Rua Dr. Roberto Frias, 4200-465, Porto, Portugal.

E-mail addresses: huu-thien.nguyen@ieee.org (H.T. Nguyen), ngocthinh.nguyen@uni-luebeck.de (N.T. Nguyen), ionela.prodan@lcis.grenoble-inp.fr (I. Prodan).

[1] Institute of Engineering and Management University Grenoble Alpes.

https://doi.org/10.1016/j.automatica.2023.111375

Most of the aforementioned work requires solving optimization sub-problems.

In this work we go further and propose a standard ellipsoid terminal invariant set under an FL controller which can be arbitrarily enlarged (subject to the state constraints that might exist), covering an arbitrarily chosen compact set containing the initial states. We show that the NMPC design achieves the *semi-global* stability property. As extensions of Nguyen (2019), we propose here two main components: (i) a method to enlarge the terminal region until it encompasses an arbitrary initial state; (ii) a formulation to easily tune the terminal region's size which directly depends on the FL controller gains and on the solution of an auxiliary Lyapunov equation.

Notations: Denote by $\boldsymbol{I}_n$ the identity matrix of size n, $0_{m\times n}$ the zero matrix of size $m \times n$, and $\mathbf{0}$ the zero matrix of appropriate dimension. Let $\lambda_{\min}(A)$, $\lambda_{\max}(A)$, and $\text{spec}(A)$ denote the minimum eigenvalue, maximum eigenvalue, and the spectrum of the square matrix A, respectively. $\mathbb{S}^n_+$ ($\mathbb{S}^n_{++}$) represents the vector space of $n \times n$ real symmetric positive semidefinite (positive definite) matrices. For a vector $\boldsymbol{x} \in \mathbb{R}^n$ and a symmetric matrix $P \in \mathbb{R}^{n\times n}$, $\|\boldsymbol{x}\|^2_P$ is the weighted norm $\boldsymbol{x}^\top P\boldsymbol{x}$ while $\|\boldsymbol{x}\|$ is the Euclidean norm. We also denote $d(x, \mathscr{Y}) = \sup\{d(x, y) : y \in \mathscr{Y}\}$ the largest distance from a point x to all points in the set $\mathscr{Y}$ and $\bar{r}_i$ is the radius of the ball $\mathscr{B}_i$. Let $[L] \triangleq [\text{diag}\{L_x, L_y, L_z\}]$ denote the diagonal matrix L with $L_x, L_y, L_z \in \mathbb{R}$ on its main diagonal. Finally, "$c(\cdot)$" and "$s(\cdot)$" denote the $\cos(\cdot)$ and $\sin(\cdot)$ functions.

2. Prerequisites

We recapitulate several contributions introduced in Nguyen et al. (2021), which are essential for the subsequent extension of the NMPC design with semi-global stability guarantees.

2.1. Multicopter feedback linearizable dynamical system

We consider the translational dynamics of a thrust-propelled vehicle system (Nguyen et al., 2020) given as follows:

$$\begin{bmatrix}\ddot{x}\\ \ddot{y}\\ \ddot{z}\end{bmatrix} = \underbrace{\begin{bmatrix}0\\0\\-g\end{bmatrix} + \begin{bmatrix}c(\phi)s(\theta)c(\psi)+s(\phi)s(\psi)\\ c(\phi)s(\theta)s(\psi)-s(\phi)c(\psi)\\ c(\phi)c(\theta)\end{bmatrix} T}_{h(\boldsymbol{u},\psi)}, \tag{1}$$

with $\boldsymbol{\xi} \triangleq [x, y, z]^\top$ the 3D position, g the gravitational acceleration, (ϕ, θ, ψ) the three Euler angles, and $T \in \mathbb{R}_+$ the input thrust (normalized by division with the quadcopter's mass).[2] The system (1) is denoted compactly as:

$$\dot{\boldsymbol{x}} = f(\boldsymbol{x}, \boldsymbol{u}), \tag{2}$$

with $\boldsymbol{x} \triangleq \left[\boldsymbol{\xi}^\top, \dot{\boldsymbol{\xi}}^\top\right]^\top \in \mathbb{R}^6$ the state vector, $\boldsymbol{u} \triangleq [T, \phi, \theta]^\top \in \mathbb{R}^3$ the input vector, and $f(\cdot) \triangleq [\dot{\boldsymbol{\xi}}^\top, h^\top(\boldsymbol{u}, \psi)]^\top$ taken from (1). The input $\boldsymbol{u}$ is subject to the saturation constraints:

$$\boldsymbol{u}(t) \in \mathscr{U} = \left\{(T, \phi, \theta) : 0 \le T \le T_{\max}, |\phi|, |\theta| \le \epsilon_{\max}\right\}, \tag{3}$$

with $T_{\max}$, $\epsilon_{\max}$ the maximum values of normalized thrust and angle. Our aim is to stabilize the dynamics (1)–(2) around their zero equilibrium point[3]:

$$\boldsymbol{x}_e = \mathbf{0}, \ \boldsymbol{u}_e = [g, 0, 0]^\top, \tag{4}$$

The system (1)–(2) admits the FL law denoted by $\boldsymbol{u}_{\text{FL}}(\mu_\xi, \psi) \triangleq [T_{\text{FL}}(\mu_\xi), \phi_{\text{FL}}(\mu_\xi, \psi), \theta_{\text{FL}}(\mu_\xi, \psi)]^\top$, with ψ the yaw angle as in (1) and $\mu_\xi \triangleq [\mu_x, \mu_y, \mu_z]^\top$ the virtual input vector (Lu et al., 2017; Nguyen et al., 2021):

$$T_{\text{FL}}(\mu_\xi) = \sqrt{\mu_x^2 + \mu_y^2 + (\mu_z + g)^2}, \tag{5a}$$

$$\phi_{\text{FL}}(\mu_\xi; \psi) = \arcsin\left(\frac{\mu_x s(\psi) - \mu_y c(\psi)}{\sqrt{\mu_x^2 + \mu_y^2 + (\mu_z + g)^2}}\right), \tag{5b}$$

$$\theta_{\text{FL}}(\mu_\xi; \psi) = \arctan\left(\frac{\mu_x c(\psi) + \mu_y s(\psi)}{\mu_z + g}\right). \tag{5c}$$

The properties of the FL law (5) are briefly recalled here:

(P1) If $\mu_z \ge -g$, the FL law (5) linearizes the nonlinear system (2) into the triplet of double integrators systems:

$$\dot{\boldsymbol{x}} = A\boldsymbol{x} + B\mu_\xi, \tag{6}$$

with $A = \begin{bmatrix}0_{3\times3} & \boldsymbol{I}_3\\ 0_{3\times3} & 0_{3\times3}\end{bmatrix}$ and $B = [0_{3\times3}, \boldsymbol{I}_3]^\top$. See the proof of Proposition 4.1 in Nguyen et al. (2020).

(P2) The input constraint admissible set w.r.t. the FL-based control $u_{\text{FL}}(\mu_\xi, \psi)$ given in (5) is as follows:

$$\mathscr{X}_{\text{FL}} = \left\{|\mu_x| \le U_x, \ |\mu_y| \le U_y, \ |\mu_z| \le U_z\right\}, \tag{7}$$

with (U_x, U_y, U_z) defined as in Proposition 4.3 from Nguyen et al. (2020). Within the admissible set $\mathscr{X}_{\text{FL}}$ (7), the FL law $\boldsymbol{u}_{\text{FL}}(\mu_\xi, \psi)$ admits a Lipschitz bound useful to prove the stability of the NMPC designs (Nguyen et al., 2021).

2.2. NMPC setup with terminal ingredients

The core requirements for designing NMPC with both the terminal cost and terminal constraint are briefed as follows (Chen & Allgöwer, 1998): (i) the terminal set being constraint admissible and positive invariant under a predefined local controller which guarantees the recursive feasibility; (ii) the closed-loop stability is established by choosing the terminal cost such that the optimal cost value becomes a Lyapunov function. For stabilizing (2) around the equilibrium point (4), an NMPC controller at time t is employed:

$$\bar{\boldsymbol{u}}_t^*(\cdot) = \arg\min_{\bar{\boldsymbol{u}}_t(\cdot)} \int_t^{t+T_p} \ell(\bar{\boldsymbol{x}}_t(s), \bar{\boldsymbol{u}}_t(s))ds + F(\bar{\boldsymbol{x}}_t(t+T_p)), \tag{8}$$

$$\text{subject to:} \quad \dot{\bar{\boldsymbol{x}}}_t = f(\bar{\boldsymbol{x}}_t, \bar{\boldsymbol{u}}_t), \tag{9a}$$

$$\bar{\boldsymbol{u}}_t(s) \in \mathscr{U}, \ s \in [t, t+T_p], \tag{9b}$$

$$\bar{\boldsymbol{x}}_t(t) = \boldsymbol{x}(t), \tag{9c}$$

$$\bar{\boldsymbol{x}}_t(t+T_p) \in \mathscr{X}_f, \tag{9d}$$

with $(\bar{\boldsymbol{x}}_t(s), \bar{\boldsymbol{u}}_t(s))$ the predicted state and input at time $s \in [t, t+T_p]$ and $\bar{\boldsymbol{u}}_t(\cdot)$ the whole predicted input trajectory. Only the solution within the first sampling time interval δ is applied, and the NMPC input is $\boldsymbol{u}(s) = \bar{\boldsymbol{u}}_t^*(s), \ \forall s \in [t, t+\delta]$. At $t+\delta$, the state is measured, time shifts $t \leftarrow t+\delta$, and (8)–(9) are repeated.

The stage cost $\ell(\cdot,\cdot)$ and terminal cost $F(\cdot)$ are defined in a standard quadratic form:

$$\ell(\boldsymbol{x}, \boldsymbol{u}) \triangleq \|\boldsymbol{x}-\boldsymbol{x}_e\|^2_Q + \|\boldsymbol{u}-\boldsymbol{u}_e\|^2_R, \ F(\boldsymbol{x}) \triangleq \|\boldsymbol{x}-\boldsymbol{x}_e\|^2_P, \tag{10}$$

with $Q \in \mathbb{S}^6_{++}$, $R \in \mathbb{S}^3_+$, weighting matrices to be defined and $P \in \mathbb{S}^6_{++}$, obtained by solving the Lyapunov equation:

$$A_K^\top P + PA_K + M = \mathbf{0}, \tag{11}$$

[2] To avoid the over-actuated control problem, the yaw angle ψ is considered an assumed known value affecting the system (as in the literature (Formentin & Lovera, 2011; Lu et al., 2017)).

[3] Taking $\boldsymbol{x}_e = \mathbf{0}$ does not reduce the generality of the analysis since the multicopter dynamics allow to hover in an arbitrary point.

where the matrix $A_K \triangleq A + BK \in \mathbb{R}^{6\times 6}$ describes the closed-loop behavior of the linear system (6):

$$\dot{\boldsymbol{x}} = (A + BK)\boldsymbol{x} = A_K\boldsymbol{x}, \tag{12}$$

with matrices A, B as in (6) and gain $K \in \mathbb{R}^{3\times 6}$ given by:

$$K = \left[\text{diag}\{K_{p_x}, K_{p_y}, K_{p_z}\}, \text{diag}\{K_{d_x}, K_{d_y}, K_{d_z}\}\right]. \tag{13}$$

All the control gains must be negative to ensure the stability of dynamics (12) by applying the controller $\boldsymbol{u}_{\text{FL}}(\mu_\xi = K\boldsymbol{x}, \psi)$ from (5) to the nonlinear dynamics (2). In the NMPC formulation (8), $\boldsymbol{u}_{\text{FL}}(K\boldsymbol{x}, \psi)$ is the *local controller*:

$$\boldsymbol{u}_{\text{loc}}(\boldsymbol{x}) \triangleq \boldsymbol{u}_{\text{FL}}(K\boldsymbol{x}, \psi), \tag{14}$$

together with the choice of the symmetric matrix $M \in \mathbb{R}^{6\times 6}$ in (11) as follows, to ensure stability and recursive feasibility of the NMPC closed-loop system:

$$M \succcurlyeq Q + \lambda_{\max}(R)(K^\top K + 2\Gamma), \tag{15}$$

with K as in (13), and $\Gamma \in \mathbb{R}^{6\times 6}$ is defined as:

$$\Gamma = \frac{1}{(-U_z + g)^2} K_{xy}^\top K_{xy}, \tag{16}$$

with $K_{xy} = \left[\text{diag}\{K_{p_x}, K_{p_y}, 0\}, \text{diag}\{K_{d_x}, K_{d_y}, 0\}\right]$ and U_z from (7). The set $\mathscr{X}_f \subset \mathbb{R}^6$ used in (9d) is the terminal invariant set derived in Nguyen et al. (2021), where we design a terminal set[4] for a discrete-time NMPC controller applied on a multicopter system:

$$\mathscr{X}_f = \{\boldsymbol{x} \in \mathbb{R}^6 : \boldsymbol{x}^\top P \boldsymbol{x} \le \delta\}, \tag{17}$$

$$\text{with } \delta = \lambda_{\min}(P) r^2,\ r^2 = \min_{q\in\{x,y,z\}} \left\{ \frac{U_q^2}{K_{p_q}^2 + K_{d_q}^2} \right\}, \tag{18}$$

with P obtained from solving (11), U_q as defined in (7) and K_{p_q}, K_{d_q} from (13). Since the semi-global stability of the NMPC scheme is a requirement in the controller design, we present next its definition and impose an additional assumption on the initial state set.

Definition 1 (*Braslavsky and Middleton (1996)*)**.** A system is **semi-globally stabilizable** to an equilibrium point $\boldsymbol{x}_e$ by means of a class $\mathscr{F}$ of feedback control laws if, for any a priori determined compact set $\mathscr{X}_0$ of initial conditions, there exists a control law in $\mathscr{F}$ that makes $\boldsymbol{x}_e$ asymptotically stable with a domain of attraction that contains $\mathscr{X}_0$.

Assumption 2. The initial states set $\mathscr{X}_0 \subset \mathbb{R}^6$ is compact and contains the state equilibrium point $\boldsymbol{x}_e$ as in (4).

3. NMPC design with terminal region enlargement

Determining the terminal set $\mathscr{X}_f$ in (17) requires solving the Lyapunov equation (11) for the matrix P with a matrix M satisfying (15). We will provide their formulations parameterized in terms of the control gains (13) and make use of them in the terminal region enlargement analysis.

3.1. Explicit solution of the lyapunov equation in (11)

We first find a parametrization of M in (15) as a function of the control gains in (13). We simplify this 6×6 matrix into a diagonal one, characterized by 6 elements which are chosen such that the condition (15) is satisfied.

[4] All the ellipsoids and balls in this paper are centered at the state equilibrium point $\boldsymbol{x}_e = \boldsymbol{0}$ as in (4).

Lemma 3. *There exist a square diagonal matrix $M \in \mathbb{S}^6_{++}$,*

$$M = \text{diag}\{m_x, m_y, m_z, m_{v_x}, m_{v_y}, m_{v_z}\}, \tag{19}$$

and a symmetric positive definite matrix $Q^* \in \mathbb{S}^6_{++}$,

$$Q^* = \begin{bmatrix} \text{diag}\{Q^*_{1_x}, Q^*_{1_y}, Q^*_{1_z}\} & \text{diag}\{Q^*_{3_x}, Q^*_{3_y}, Q^*_{3_z}\} \\ \text{diag}\{Q^*_{3_x}, Q^*_{3_y}, Q^*_{3_z}\} & \text{diag}\{Q^*_{2_x}, Q^*_{2_y}, Q^*_{2_z}\} \end{bmatrix}, \tag{20}$$

where Q^* represents the right-hand side of (15), i.e.,

$$Q^* \triangleq Q + \lambda_{max}(R)(K^\top K + 2\Gamma), \tag{21}$$

satisfying $M \succcurlyeq Q^* \succ \boldsymbol{0}$. □

Proof. By calculating $\lambda_{\max}(R)$ of R in (10) and directly replacing K in (13), Γ in (16), Q in (10) into the right-hand side of (15), Q^* has the symmetric form as in (20). Since $\text{spec}(K^\top K) = \{0, 0, 0, K_{p_x}^2 + K_{d_x}^2, K_{p_y}^2 + K_{d_y}^2, K_{p_z}^2 + K_{d_z}^2\}$, $K^\top K \succcurlyeq \boldsymbol{0}$. Similarly, with $\text{spec}(K_{xy}^\top K_{xy}) = \{0, 0, 0, 0, K_{p_x}^2 + K_{d_x}^2, K_{p_y}^2 + K_{d_y}^2\}$, $K_{xy}^\top K_{xy} \succcurlyeq \boldsymbol{0}$, which leads to $\Gamma \succcurlyeq \boldsymbol{0}$. With $R \succcurlyeq \boldsymbol{0}$ in (10), $\lambda_{\max}(R) \ge 0$, hence $\lambda_{\max}(R)(K^\top K + 2\Gamma) \succcurlyeq \boldsymbol{0}$. Combining with $Q \succ \boldsymbol{0}$ in (10), $Q^* \succ \boldsymbol{0}$. Finally, we examine the positive semi-definiteness of the matrix $(M - Q^*)$ by considering the quadratic form $\boldsymbol{x}^\top(M - Q^*)\boldsymbol{x}$ with M in (19), Q^* in (20) and an arbitrary vector $\boldsymbol{x} = [x, y, z, v_x, v_y, v_z]^\top \in \mathbb{R}^6$: $\boldsymbol{x}^\top(M - Q^*)\boldsymbol{x} = \sum_{q\in\{x,y,z\}}[(m_q - Q^*_{1_q})q^2 + (m_{v_q} - Q^*_{2_q})v_q^2 - 2Q^*_{3_q} q v_q] \ge 0$. This is verified by simultaneously guaranteeing each individual quadratic form to be non-negative:

$$(m_q - Q^*_{1_q})q^2 + (m_{v_q} - Q^*_{2_q})v_q^2 - 2Q^*_{3_q} q v_q \ge 0, \forall q \in \{x, y, z\}. \tag{22}$$

From Gantmacher (1960), a quadratic form is positive semidefinite iff the principal minors of its coefficient matrix are non-negative, so the condition (22) is satisfied by imposing:

$$m_q - Q^*_{1_q} \ge 0,\ m_{v_q} - Q^*_{2_q} \ge 0,\ (m_q - Q^*_{1_q})(m_{v_q} - Q^*_{2_q}) \ge Q^{*2}_{3_q}, \tag{23}$$

$\forall q \in \{x, y, z\}$. Moreover, the entries on main diagonal of $Q^* \succ \boldsymbol{0}$ are also positive, i.e. $\{Q^*_{1_q}, Q^*_{2_q} > 0 : q \in \{x, y, z\}\}$. Therefore, a choice for M which satisfies (23) is:

$$m_q \ge Q^*_{1_q} + |Q^*_{3_q}| > 0,\ \ m_{v_q} \ge Q^*_{2_q} + |Q^*_{3_q}| > 0, \forall q \in \{x, y, z\}. \tag{24}$$

This completes the proof. □

Next, we show that with the terminal set $\mathscr{X}_f$ as in (17)–(18), the matrix M as in (19), and the terminal weighting matrix P satisfying (11), the NMPC scheme (8)–(9) is recursively feasible and the dynamics (12) are asymptotically stable.

Lemma 4. *The terminal set $\mathscr{X}_f$ in (17) is forward invariant in the continuous-time domain. Moreover, the recursive feasibility of the NMPC scheme and the asymptotic stability of the closed-loop dynamics are guaranteed with the choices of P and M satisfying (11), (15).* □

Proof. Consider the Lyapunov function $V = \boldsymbol{x}^\top P \boldsymbol{x}$. Since $P \succ \boldsymbol{0}$, $V > 0$. Next, $\dot{V} = \boldsymbol{x}^\top(A_K^\top P + P A_K)\boldsymbol{x} = -\boldsymbol{x}^\top M \boldsymbol{x} < 0$, since $M \succ \boldsymbol{0}$ as in Lemma 3, hence, $\mathscr{X}_f$ is forward invariant. Moreover, $\frac{d}{dt}F(f(\boldsymbol{x})) + \ell(\boldsymbol{x}, \boldsymbol{u}_{\text{loc}}(\boldsymbol{x})) \le \boldsymbol{x}^\top(A_K^\top P + P A_K)\boldsymbol{x} + \boldsymbol{x}^\top Q^* \boldsymbol{x} = \boldsymbol{x}^\top(-M + Q^*)\boldsymbol{x} \le 0$, since $M \succcurlyeq Q^*$ as proven in Lemma 3, with Q^* as in (21), which verifies the asymptotic stability. The proof is complete. □

Having obtained a parametrization of the matrix M in terms of Q^* as in (20), we solve the full rank Lyapunov equation (11) to obtain the matrix P. In order to do so, notice that A_K and M both have the form of a 6×6 square matrix composed of four blocks of 3×3 diagonal matrices, hence, we choose the matrix P to be also a square matrix composes of blocks of diagonal matrix, then we perform block matrix manipulations to find P and prove that P is positive definite.

Proposition 5. *The solution of the Lyapunov equation (11) is defined as a symmetric positive definite matrix:*

$$P \triangleq \begin{bmatrix} [P_1] & [P_3] \\ [P_3] & [P_2] \end{bmatrix} = \begin{bmatrix} \mathrm{diag}\{P_{1_x}, P_{1_y}, P_{1_z}\} & \mathrm{diag}\{P_{3_x}, P_{3_y}, P_{3_z}\} \\ \mathrm{diag}\{P_{3_x}, P_{3_y}, P_{3_z}\} & \mathrm{diag}\{P_{2_x}, P_{2_y}, P_{2_z}\} \end{bmatrix}, \quad (25)$$

whose entries are given by:

$$P_{1_q} = \frac{1}{2}\left(\frac{K_{d_q}}{K_{p_q}} - \frac{1}{K_{d_q}}\right) m_q + \frac{K_{p_q}}{2K_{d_q}} m_{v_q}, \quad (26a)$$

$$P_{2_q} = \frac{m_q}{2K_{p_q}K_{d_q}} - \frac{m_{v_q}}{2K_{d_q}}, \quad (26b)$$

$$P_{3_q} = -\frac{m_q}{2K_{p_q}}, \quad (26c)$$

with K_{p_q}, K_{d_q} in (13), m_q, m_{v_q} in (19) for $q \in \{x, y, z\}$. □

Proof. By replacing $A_K = \begin{bmatrix} \mathbf{0} & \boldsymbol{I}_3 \\ [K_p] & [K_d] \end{bmatrix}$, $M = \begin{bmatrix} [m] & \mathbf{0} \\ \mathbf{0} & [m_v] \end{bmatrix}$ in (19), and $P = \begin{bmatrix} [P_1] & [P_3] \\ [P_3] & [P_2] \end{bmatrix}$ in (25) into (11), exploiting the element-wise matrix multiplication (denoted by $\circ$) on blocks of diagonal matrices, and reorganizing the terms, we attain:

$$2[K_p] \circ [P_3] + [m] = \mathbf{0}, \quad (27a)$$

$$[P_1] + [K_p] \circ [P_2] + [K_d] \circ [P_3] = \mathbf{0}, \quad (27b)$$

$$2[P_3] + 2[K_d] \circ [P_2] + [m_v] = \mathbf{0}, \quad (27c)$$

which can be further simplified to a matrix equation:

$$\begin{bmatrix} \mathbf{0} & \mathbf{0} & 2[K_p] \\ \mathbf{0} & 2[K_d] & 2\boldsymbol{I}_3 \\ \boldsymbol{I}_3 & [K_p] & [K_d] \end{bmatrix} \begin{bmatrix} \boldsymbol{P}_1 \\ \boldsymbol{P}_2 \\ \boldsymbol{P}_3 \end{bmatrix} = - \begin{bmatrix} \boldsymbol{m} \\ \boldsymbol{m_v} \\ \mathbf{0} \end{bmatrix}, \quad (28)$$

where $\boldsymbol{P_i} \triangleq [P_{i_x}, P_{i_y}, P_{i_z}]^\top$ for $i \in \{1, 2, 3\}$, $\boldsymbol{m} \triangleq [m_x, m_y, m_z]^\top$, and $\boldsymbol{m_v} \triangleq [m_{v_x}, m_{v_y}, m_{v_z}]^\top$. Then, the condition $K_{p_q}, K_{d_q} < 0$ for $q \in \{x, y, z\}$ entails that the square matrix on the left-hand side of (28) is full rank, hence, (28) has a unique solution. By solving (28) for nine unknown variables $\{P_{1_q}, P_{2_q}, P_{3_q} : q \in \{x, y, z\}\}$, we obtain (26). □

3.2. Eigenvalues of the matrix P

After obtaining the parametrization of the matrix P as in (25)–(26), we provide its eigenvalues since they will be employed to expand the terminal invariant set $\mathscr{X}_f$ and be used to verify if the matrix P is positive definite. Moreover, as we demonstrate hereinafter, the size of the terminal set is also determined by the feedback gains K_{p_q}, K_{d_q} in (13).

Lemma 6. *The spectrum of the matrix $P \in \mathbb{S}^6_{++}$ as in (25) composes of six positive eigenvalues:*

$$\mathrm{spec}(P) = \{\lambda_{1_q}, \lambda_{2_q} : q \in \{x, y, z\}\}, \quad (29)$$

where each pair of eigenvalues is explicitly given by:

$$\{\lambda_{1_q}, \lambda_{2_q}\} = \left\{\frac{1}{2}\left(P_{1_q} + P_{2_q} \pm \sqrt{(P_{1_q} - P_{2_q})^2 + 4P_{3_q}^2}\right)\right\}, \quad (30)$$

and $\{P_{1_q}, P_{2_q}, P_{3_q} : q \in \{x, y, z\}\}$ are from (26). □

Proof. Since P is a real symmetric matrix, define $\lambda \in \mathbb{R}$ an eigenvalue of P. Therefore, λ satisfies the characteristic equation $\det(P - \lambda \boldsymbol{I}_6) = 0$. Expanding this constraint, we attain the system of equations: $\lambda^2 \boldsymbol{I}_3 - \lambda([P_1] + [P_2]) + ([P_1] \circ [P_2] - [P_3] \circ [P_3]) = \mathbf{0}$, which can be explicitly written as a set of three equality constraints:

$$\left\{\lambda^2 - \lambda(P_{1_q} + P_{2_q}) + (P_{1_q}P_{2_q} - P_{3_q}^2) = 0 : q \in \{x, y, z\}\right\}. \quad (31)$$

By solving (31) for λ, we obtain (30). Now applying the Vieta's formula for the quadratic polynomial on the left-hand side of (31), the pair $\{\lambda_{1_q}, \lambda_{2_q}\}$ satisfies $\lambda_{1_q} + \lambda_{2_q} = P_{1_q} + P_{2_q} = \frac{m_q(K_{d_q}^2 - K_{p_q}+1) + m_{v_q}(K_{p_q}^2 - K_{p_q})}{2K_{p_q}K_{d_q}} > 0$, $\lambda_{1_q}\lambda_{2_q} = P_{1_q}P_{2_q} - P_{3_q}^2 = \frac{-m_q^2 + m_q m_{v_q}(2K_{p_q} - K_{d_q}^2) - m_{v_q}^2 K_{p_q}^2}{4K_{p_q}K_{d_q}^2} > 0$ with $K_{p_q}, K_{d_q} < 0$ in (13), $m_q, m_{v_q} > 0$ in (24). Hence, λ_{1_q} and λ_{2_q} are positive. □

3.3. Terminal region enlargement

Now, we show that the size of the terminal set $\mathscr{X}_f$ in (9d) depends on the matrix P in (25) and its eigenvalues in (30), which in turn depends on the feedback gains K_{p_q}, K_{d_q} in (13) of the FL local controller (14). Therefore, by tuning the control gains K_{p_q}, K_{d_q}, we change the size of the terminal set. This subsection presents a method of increasing the terminal set such that it covers the set of feasible initial states.

We may enlarge the ellipsoid $\mathscr{X}_f$ as in (17) by increasing its semi-axes' length (i.e., $\sqrt{\lambda_i(P/\delta)}$ with $i \in \{1, \ldots, 6\}$) . However, the directions of the semi-axes also depend on the eigenvectors of the matrix P/δ, and they are complicated to manipulate. Therefore, we will increase the size of the ellipsoid terminal invariant set $\mathscr{X}_f$ through increasing the radius of the ball inscribed in the ellipsoid. To do so, we define the auxiliary notion of a *terminal ball*:

$$\mathscr{B}_f = \left\{\boldsymbol{x} \in \mathbb{R}^6 \mid \|\boldsymbol{x}\|^2 \le \bar{r}^2\right\}, \text{ with } \bar{r}^2 \triangleq \frac{\lambda_{\min}(P)}{\lambda_{\max}(P)} r^2, \quad (32)$$

where r as in (18), and come to the following Lemma.

Lemma 7. *The terminal ball $\mathscr{B}_f$ as in (32) is inscribed in the ellipsoid $\mathscr{X}_f$ defined as in (17)–(18), i.e., $\mathscr{B}_f \subseteq \mathscr{X}_f$.* □

Proof. For $\boldsymbol{x} \in \mathscr{B}_f$, from (32), $\lambda_{\max}(P)\|\boldsymbol{x}\|^2 \le \lambda_{\min}(P) r^2$, Now, using the Rayleigh quotient which gives a relation between the $P-$weighted norm and the Euclidean norm of a vector $\boldsymbol{x} \in \mathbb{R}^6$: $\|\boldsymbol{x}\|_P^2 \le \lambda_{\max}(P)\|\boldsymbol{x}\|^2$, we obtain the chain of inequalities: $\|\boldsymbol{x}\|_P^2 \le \lambda_{\max}(P)\|\boldsymbol{x}\|^2 \le \lambda_{\min}(P) r^2$, which leads to the inclusion $\mathscr{B}_f \subseteq \mathscr{X}_f$ and completes the proof. □

Observe that the radius of the terminal ball $\mathscr{B}_f$ in (32) depends on the smallest and largest eigenvalues of the matrix P, without loss of generality, the following assumption is made to pave the way for the terminal set enlargement.

Assumption 8. The feedback control gains K_{p_q}, K_{d_q} in (13) and m_q, m_{v_q} in (19), have the same values regardless of q:

$$K_{p_q} \triangleq k_p, \; K_{d_q} \triangleq k_d, \; m_q \triangleq m_1, \; m_{v_q} \triangleq m_2. \quad (33)$$

With Assumption 8, the three pairs of eigenvalues $\{\lambda_{1_q}, \lambda_{2_q}\}$ as in (30) are equal for $q \in \{x, y, z\}$ Furthermore, the minimum and maximum eigenvalues of P in (25) are also equal to the minimum and maximum eigenvalues in each pair:

$$\lambda_{\min}(P) = \min_{q \in \{x,y,z\}} \{\lambda_{1_q}, \lambda_{2_q}\}, \; \lambda_{\max}(P) = \max_{q \in \{x,y,z\}} \{\lambda_{1_q}, \lambda_{2_q}\}. \quad (34)$$

Using this simplification, we present next the feasibility of the terminal set enlargement.

Proposition 9. *The radius of the ball $\mathscr{B}_f$ in (32) can be enlarged to infinity with appropriate feedback gains K_{p_q}, K_{d_q} from (13) and the matrix M in (19) satisfying Assumption 8.* □

Proof. From the simplification (33) and its consequence (34), the smallest and largest eigenvalues of matrix P are obtained by

replacing (26) to (30) and explicitly expressed as in (35).

$$\lambda_{\substack{min\\max}}(P) = \frac{1}{4}\left\{\left(\frac{k_d}{k_p} - \frac{1}{k_d} + \frac{1}{k_p k_d}\right)m_1 + \left(\frac{k_p - 1}{k_d}\right)m_2 \mp \sqrt{\left[\left(\frac{k_d}{k_p} - \frac{1}{k_d} - \frac{1}{k_p k_d}\right)m_1 + \left(\frac{k_p + 1}{k_d}\right)m_2\right]^2 + \frac{4}{k_p^2}m_1^2}\right\}. \tag{35}$$

Next, define $\sigma \triangleq m_1/m_2$, then from the condition of m_1, m_2 in Lemma 3, $\sigma > 0$. Further, let us define the function $\gamma_{\mp}(k_p, k_d, \sigma) \triangleq \left(k_d^2 - k_p + 1\right)\sigma + k_p^2 - k_p \mp \sqrt{\left[\left(k_d^2 - k_p - 1\right)\sigma + k_p^2 + k_p\right]^2 + 4k_d^2\sigma^2}$, which is the numerator of $\lambda_{\substack{min\\max}}(P)$ in (35) when the common denominator is $4k_pk_d$, hence, the radius $\bar{r}$ of the ball $\mathscr{B}_f$ in (32) satisfies:

$$\bar{r}^2 = \frac{\gamma_-(k_p, k_d, \sigma)}{\gamma_+(k_p, k_d, \sigma)} r^2, \tag{36}$$

where $\lim_{(k_p,k_d)\to(0^-,0^-)} \gamma_+^2(k_p, k_d, \sigma) = 4\sigma^2$. Therefore, by replacing r^2 in (18), under Assumption 8, $r^2 = \frac{U_{\min}^2}{k_p^2+k_d^2}$ with $U_{\min}^2 \triangleq \min_{q\in\{x,y,z\}}\left\{U_q^2\right\}$ to (36), we obtain the limit of $\bar{r}^2$ as k_p, k_d approach zero from negative as $\lim_{(k_p,k_d)\to(0^-,0^-)} \bar{r}^2 = \lim_{(k_p,k_d)\to(0^-,0^-)} \frac{-\sigma k_d^2 k_p - k_p^3 + 2k_p^2\sigma - k_p\sigma^2}{\sigma^2(k_p^2+k_d^2)} U_{\min}^2$, where $-\sigma k_d^2 k_p - k_p^3 + 2k_p^2\sigma > 0$, and $\lim_{(k_p,k_d)\to(0^-,0^-)} \frac{-k_p}{k_p^2+k_d^2} = +\infty$ when $k_d^2 \to 0$ faster than $k_p \to 0^-$. Hence, the proof is complete. □

Proposition 10. *Suppose that Assumption 2 and Assumption 8 are satisfied, the ellipsoid $\mathscr{X}_f$ as in (17)–(18) can be served as the terminal set for the NMPC problem (8)–(16) to achieve the semi-globally asymptotic stability.* □

Proof. The radius of the terminal ball $\mathscr{B}_f$ is easily enlarged by changing the control gains k_p, k_d, which leads to the enlargement of the terminal set $\mathscr{X}_f$ to cover any feasible initial states. With Assumption 2 and its result in Proposition 9, there always exists a ball covering the set of initial states $\mathscr{X}_0$. Since the terminal ball is centered at the state equilibrium $\boldsymbol{x}_e = \mathbf{0}$ defined in (4), the semi-globally asymptotic stability of the NMPC controller is guaranteed by ensuring that the radius of the terminal ball larger than or equal to the largest norm of all points belonging to the set $\mathscr{X}_0$:

$$\bar{r} \geq r_0 \triangleq d(\boldsymbol{x}_e, \mathscr{X}_0), \tag{37}$$

which completes the proof. □

3.4. NMPC design procedure

After gathering all the necessary ingredients for the calculation of the terminal set, we present in Algorithm 1 the procedure to design an NMPC controller with semi-globally asymptotic stability.

Algorithm 1 NMPC design with semi-globally asymptotic stabilization

data The compact set $\mathscr{X}_0$ contains the equilibrium state $\boldsymbol{x}_e$, U_q ($q \in \{x, y, z\}$) in (7)
Calculate $r_0 = d(\boldsymbol{x}_e, \mathscr{X}_0)$ as in (37)
Choose $Q \in \mathbb{S}_{++}^6$, $R \in \mathbb{S}_{+}^3$ in (10)
Construct K in (13), calculate Γ in (16) by solving $\bar{r} \geq r_0$ for $k_p, k_d < 0$ in (33), with:
function $\bar{r}$ =COMPUTE_R_BAR(k_p, k_d)
  Calculate $Q^* = Q + \lambda_{\max}(R)(K^\top K + 2\Gamma)$ in (21)
  Specify $M \succcurlyeq Q^*$ in (15) satisfying (24) and (33)
  Determine P in the terminal cost (10) following (26)
  Calculate $r^2 = \min_{q\in\{x,y,z\}}\left\{\frac{U_q^2}{k_p^2+k_d^2}\right\}$ in (18)
  Calculate the radius of $\mathscr{B}_f$ in (32): $\bar{r}^2 = \frac{\lambda_{\min}(P)}{\lambda_{\max}(P)} r^2$
end function
Construct the terminal set $\mathscr{X}_f$ in (9d) using (17)
return P, $\mathscr{X}_f$
Choose the MPC prediction horizon T_P in (8) which guarantees the recursive feasibility
Solve the optimization problem (8)
result NMPC solution $\bar{\boldsymbol{u}}_t^*$ in (8)

4. Illustrative examples

This section validates the NMPC design with the terminal region enlargement through simulations. While the proposed approach shows robust promise for experimental implementation, in this paper we concentrate only on providing the necessary ingredients for theoretical guarantees. The simulations are done on the Crazyflie quadcopter platform with the input constraint $\mathscr{U}$ in (3) chosen as follows:

$$\mathscr{U} = \left\{0 \leq T \leq 2\,g,\ |\phi| \leq 10^\circ,\ |\theta| \leq 10^\circ\right\}, \tag{38}$$

the ψ angle is fixed as zero, and the input constraint (7) $U_q = 1.0875\ \forall q \in \{x, y, z\}$ (Nguyen et al., 2021). For comparing the performance of our proposed Algorithm 1, we consider the qsMPC approach in Chen and Allgöwer (1998), which makes use of a linear local controller $\boldsymbol{u}_{qs} = K_{qs}(\boldsymbol{x} - \boldsymbol{x}_e) + \boldsymbol{u}_e$ to linearize the dynamics (2) inside the terminal set as:

$$\dot{\boldsymbol{x}} = A_{K_{qs}}\boldsymbol{x}. \tag{39}$$

4.1. Simulation setup

The following three scenarios are established to evaluate our proposed terminal set construction and enlargement approach. We utilize the subscript ${}_i\square$, with $i \in \{1, 2, 3\}$ for the equivalent scenario.

Scenario 1 (qsMPC) follows the procedure in Chen and Allgöwer (1998, Section 3). The feedback gain matrix K_{qs} is designated as follows:

$$K_{qs} = \begin{bmatrix} 0 & 0 & k_p & 0 & 0 & k_d \\ \frac{k_p}{g}s(\psi) & -\frac{k_p}{g}c(\psi) & 0 & \frac{k_d}{g}s(\psi) & -\frac{k_d}{g}c(\psi) & 0 \\ \frac{k_p}{g}c(\psi) & \frac{k_p}{g}s(\psi) & 0 & \frac{k_d}{g}c(\psi) & \frac{k_d}{g}s(\psi) & 0 \end{bmatrix}, \tag{40}$$

such that the matrix $A_{K_{qs}}$ in (39) is the same as A_K in (12), i.e., the eigenvalues of the corresponding closed-loop dynamics are similar, so that our comparison is meaningful. We choose ${}_1k_p = {}_1k_d = -2$ which induces $\lambda_{\max}(A_{K_{qs}}) = -1$ and leads to the choice of $\kappa = 0.95$. We then solve for the terminal weighting matrix as:

$${}_1P = \begin{bmatrix} \text{diag}\{304.8837, 304.8837, 342.4938\} & \text{diag}\{147.3301, 147.3301, 166.1845\} \\ \text{diag}\{147.3301, 147.3301, 166.1845\} & \text{diag}\{145.0961, 145.0961, 164.9377\} \end{bmatrix},$$

and find $\alpha = 0.0687$. The terminal set in this scenario is ${}_1\mathscr{X}_f = \{\boldsymbol{x} \in \mathbb{R}^6 : \boldsymbol{x}^\top({}_1P)\boldsymbol{x} \leq \alpha\}$.

Scenario 2 (the initial state **outside** the terminal set) mimics our work in Nguyen et al. (2021). The feedback gains are similar to scenario 1, ${}_2k_p = {}_2k_d = -2$ in (13), which makes the radius of the ball $\mathscr{B}_f$ in (32) ${}_2\bar{r} = 0.2045$ (${}_2r = 0.3845$). We intentionally choose the initial state $\boldsymbol{x}_0 = [0.3, -0.4, 0.5, 0, 0, 0]^\top$ to be numerically and visually *outside* the terminal set ${}_2\mathscr{X}_f$. Hence, $r_0 = d(\boldsymbol{x}_e, \mathscr{X}_0) = \|\boldsymbol{x}_0 - \boldsymbol{x}_e\| = \|\boldsymbol{x}_0\| = 0.7071$.

Scenario 3 (the initial state **inside** the terminal set) follows our Algorithm 1. Here, we reduce k_p, k_d (13) until the radius $\bar{r}$ of the ball $\mathscr{B}_f$ in (32) larger than r_0 in scenario 2 to make the initial state *inside* the terminal set ${}_3\mathscr{X}_f$, satisfying (37), which leads to the choice ${}_3k_p = {}_3k_d = -0.75$ and the radius ${}_3\bar{r} = 0.7111$ (${}_3r = 1.0253$). The terminal sets in scenarios 2 and 3 are ${}_i\mathscr{X}_f = \{\boldsymbol{x} \in \mathbb{R}^6 : \boldsymbol{x}^\top ({}_iP)\boldsymbol{x} \le \lambda_{\min}({}_iP)\,{}_ir^2\}$ for $i \in \{2, 3\}$.

For all three scenarios, the simulation length is chosen as 6*s*. The optimal control problem (8) is transformed to a nonlinear programming problem and is solved using the Direct Multiple Shooting method (Bock & Plitt, 1984) in CasADi (Andersson et al., 2019) with solver IPOPT (Wächter & Biegler, 2006). The initial guesses for the solver are $(\boldsymbol{x}_e, \boldsymbol{u}_e)$. Each NMPC iteration $[t, t+T_p]$ is split into T_p/δ arcs, $t_0 = t, t_1, \ldots, t_{T_p/\delta} = t + T_p$, with δ the sampling time in Section 2. In each arc $[t_i, t_{i+1}]$, $i \in \{1, \ldots, T_p/\delta - 1\}$, the input is kept constant, while the final state at t_{i+1} is derived from (2) using the Runge Kutta 4*th* order method with step size $\delta = 0.1$ and the initial condition at t_i constrained to be the final state of the previous interval $[t_{i-1}, t_i]$, whereas the initial condition at t_0 is $\boldsymbol{x}_0$. The ellipsoidal terminal sets are plotted with MPT3 toolbox (Herceg et al., 2013), while their volumes are calculated using CORA (Gaßmann & Althoff, 2022). The simulations are done on a lab computer with an AMD Ryzen 5 2600 6-core processor, 3.4*GHz*, 12 CPUs, 16*GB* RAM, Python 3.8.5.

The sampling time δ in Section 2 is chosen as 0.1*s*. For the prediction horizon T_p, we choose the minimum length such that the problem attains the feasibility property, i.e., the first MPC iteration is solvable. Since the terminal set ${}_3\mathscr{X}_f$ in scenario 3 already contains the initial state, the shortest T_p, ${}_3T_p = 0.2s$ (2 steps) is chosen. For scenario 2, the minimum T_p to guarantee the recursive feasibility is ${}_2T_p = 1.1s$, while ${}_1T_p = 1.9s$ for the qsMPC with a small size ellipsoid.

Remark 11. Assumption 8 only makes $Q^*_{1_x} = Q^*_{1_y} > Q^*_{1_z}$, $Q^*_{2_x} = Q^*_{2_y} > Q^*_{2_z}$, and $Q^*_{3_x} = Q^*_{3_y} > Q^*_{3_z}$ with $k_p, k_d < 0$, $R \in \mathbb{S}^3_+$, $Q \in \mathbb{S}^6_{++}$ in (10), hence, the condition for the matrix M in (24) with the simplification (33) is augmented to:

$$m_1 \ge \max_{q\in\{x,y,z\}}\{Q^*_{1_q} + |Q^*_{3_q}|\},\ m_2 \ge \max_{q\in\{x,y,z\}}\{Q^*_{2_q} + |Q^*_{3_q}|\}. \quad (41)$$

We choose Q, R in (10) to be $10\boldsymbol{I}_6$, $\boldsymbol{I}_3$ for the three scenarios. For scenario 2, $\max_{q\in\{x,y,z\}}\{Q^*_{1_q} + |Q^*_{3_q}|\} = \max_{q\in\{x,y,z\}}\{Q^*_{2_q} + |Q^*_{3_q}|\} = 18.2103$, hence, we choose ${}_2M = \mathrm{diag}\{20\boldsymbol{I}_3, 30\boldsymbol{I}_3\}$, while in scenario 3, $\max_{q\in\{x,y,z\}}\{Q^*_{1_q} + |Q^*_{3_q}|\} = \max_{q\in\{x,y,z\}}\{Q^*_{2_q} + |Q^*_{3_q}|\} = 11.1546$, we choose ${}_3M = \mathrm{diag}\{20\boldsymbol{I}_3, 30\boldsymbol{I}_3\}$. Therefore, following (26), we obtain ${}_2P = \begin{bmatrix} 30\boldsymbol{I}_3 & 5\boldsymbol{I}_3 \\ 5\boldsymbol{I}_3 & 10\boldsymbol{I}_3 \end{bmatrix}$ and ${}_3P = \begin{bmatrix} 38.(3)\boldsymbol{I}_3 & 13.(3)\boldsymbol{I}_3 \\ 13.(3)\boldsymbol{I}_3 & 37.(7)\boldsymbol{I}_3 \end{bmatrix}$.

4.2. Comparisons and discussions

The simulation results are shown in Figs. 1–5. Since the three NMPC controllers have the same weighting matrices Q, R in the stage cost, the performance of these controllers boils down to three major factors: the terminal cost weighting matrix P, the size of the terminal set $\mathscr{X}_f$, and the prediction horizon T_p. In Fig. 1, for each scenario, we plot the convex hull of the projections of the three ellipsoids ${}_i\mathscr{X}_f$ onto the $(q - v_q)$ plans, for $i \in \{1, 2, 3\}$ and $q \in \{x, y, z\}$, following the steps in Karl et al. (1994, Section 3). We also show the state trajectories $v_{q_i} - q_i$ with $q \in \{y, z\}$ and $i \in \{1, 2, 3\}$. The terminal set ${}_1\mathscr{X}_f$ in scenario 1 is the green ellipsoid that can only be easily seen with a 6x zoom. The ellipsoid in scenario 2 is the red ellipsoid that does not cover the initial state. By just decreasing the control gains k_p, k_d, the red ellipsoid becomes the large blue ellipsoid in scenario 3. Our approaches provide larger ellipsoid terminal sets: the terminal set in scenario 2 ($vol({}_2\mathscr{X}_f) = 25 \times 10^{-4}$) is $\simeq 5.7 \times 10^6$ times larger than the qsMPC terminal set ($vol({}_1\mathscr{X}_f) = 4.3766 \times 10^{-10}$), and by simply reducing the control gains from scenario 2 to scenario 3, the ellipsoid is $\simeq 801$ times larger ($vol({}_3\mathscr{X}_f) = 2.0028$).

The change of the position (x, y, z) are in Fig. 2, and the velocity (v_x, v_y, v_z) are in Fig. 3. We choose the 2% settling time (t_s) criteria to evaluate the convergence and gather the results

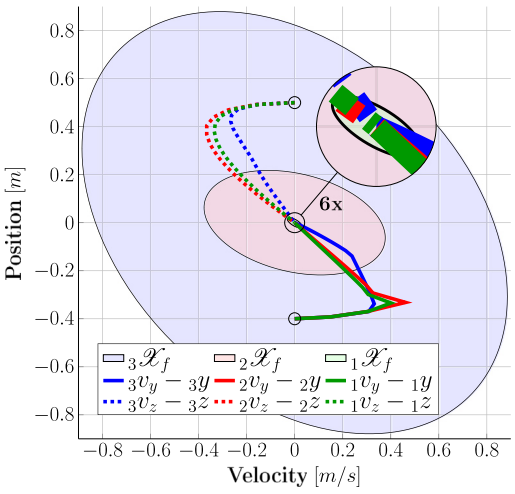

Fig. 1. The trajectories projected onto the $y - z$ plane.

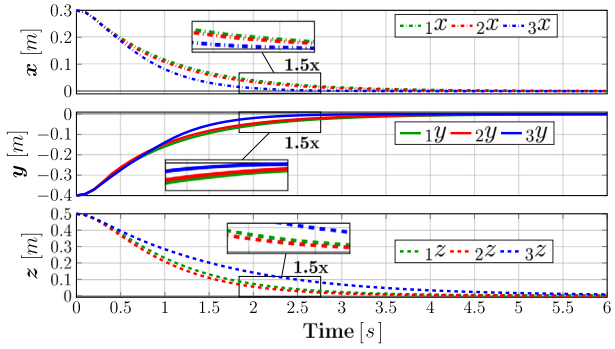

Fig. 2. Multicopter actual motion for the 3 scenarios.

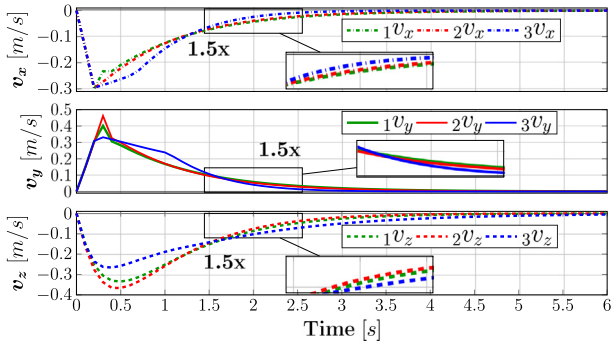

Fig. 3. Multicopter velocity for the 3 scenarios.

Table 1
The settling time (t_s $[s]$) for each state in the 3 scenarios.

	x	y	z	v_x	v_y	v_z
Scenario 1	2.7	3	3.1	2.8	3.1	3.3
Scenario 2	2.5	2.8	2.8	2.6	2.9	3.0
Scenario 3	1.8	2	4.7	2.1	2.4	4.3

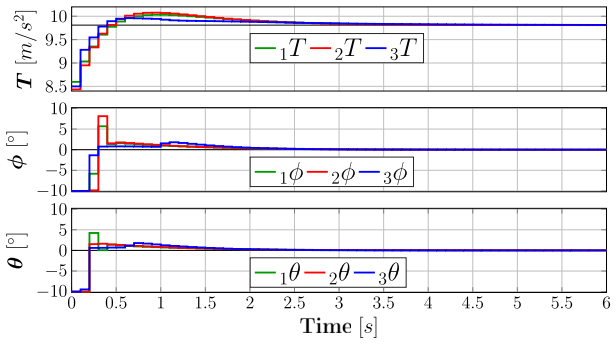

Fig. 4. Multicopter control inputs for the 3 scenarios.

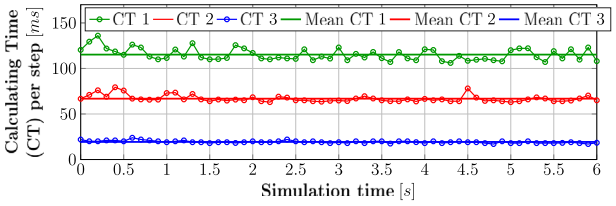

Fig. 5. Calculating time in the 3 scenarios.

in Table 1. For all 6 states, although scenario 1 has the same feedback control gains as scenario 2 ($k_p = k_d = -2$), scenario 2 provides a faster convergence with its shorter T_p. On the other hand, scenario 3 gives the fastest rate for x, y, v_x, v_y, but the slowest for z and v_z, despite the initial state is already inside the terminal set and the T_p in scenario 3 is the shortest. The control inputs are in Fig. 4, satisfying the input constraint (38), which are implicitly imposed in the choice of U_q ($q \in \{x, y, z\}$).

An energy consumption function along the simulation horizon, $E = \int_{t_{\text{init}}=0\text{s}}^{t_{end}=6\text{s}} T^2\, dt$, where T is the normalized thrust applied to the Crazyflie, is employed to quantitatively compare the controllers. The quadcopter spends the least energy in scenario 3 ($_3E = 588.3076\ \text{m}^2/\text{s}^3$) because it is already inside the terminal invariant set from the beginning, while $_1E = 588.6654$ and $_2E = 588.9833\ (\text{m}^2/\text{s}^3)$. The calculating time (CT), i.e., the time needed to solve (8), and the mean CT per step, are shown in Fig. 5. The qsMPC takes 115 ms per step in average, higher than the sampling time $\delta = 100$ ms, while scenario 2 reduces this to 67 ms. With the advantage of reducing the prediction horizon T_p to 2 steps, scenario 3 has the shortest CT per step, 19 ms.

5. Conclusions

This brief paper presents an NMPC design with semi-globally asymptotic stability for a multicopter, accomplished by demonstrating the flexibility in enlarging the size of the terminal invariant set only by changing the feedback linearization control gains. This technique shows potential in real-time implementation, where onboard computing time is critical. Future work will focus on finding time-varying, optimal size terminal sets that balance the performance of the NMPC scheme and the online computation time.

Acknowledgments

The authors are grateful for the contributions of Prof. Fernando Lobo Pereira during several stages of this research. This work has been partially supported by the PHC Alliance Hubert Curien Programme, France (PHC PESSOA, Projet no. 47913XD), La Région, Pack Ambition Recherche 2021 - PlanMAV and by the French National Research Agency, France in the framework of the "Investissements d'avenir" program "ANR-15-IDEX-02" and the LabEx PERSYVAL, France "ANR-11-LABX-0025-01". Huu Thien Nguyen is supported by FCT/MCTES (PIDDAC), Portugal under grants 2020.07959.BD, 2021.09306.CBM, 2022.02801.PTDC, LA/P/0112/2020, UIDB/00147/2020, UIDP/00147/2020. Ngoc Thinh Nguyen is funded by the German Ministry of Food and Agriculture (BMEL) Project No. 28DK133A20.

References

Alamir, Mazen (2018). Stability proof for nonlinear MPC design using monotonically increasing weighting profiles without terminal constraints. *Automatica*, *87*, 455–459.

Andersson, Joel A. E., Gillis, Joris, Horn, Greg, Rawlings, James B., & Diehl, Moritz (2019). CasADi: A software framework for nonlinear optimization and optimal control. *Mathematical Programming Computation*, *11*(1), 1–36.

Bock, H. G., & Plitt, K. J. (1984). A multiple shooting algorithm for direct solution of optimal control problems. *IFAC Proceedings Volumes*, *17*(2), 1603–1608.

Braslavsky, J. H., & Middleton, R. H. (1996). Global and semi-global stabilizability in certain cascade nonlinear systems. *IEEE Transactions on Automatic Control*, *41*(6), 6.

Brunner, Florian D., Lazar, Mircea, & Allgower, Frank (2013). Stabilizing linear model predictive control: On the enlargement of the terminal set. In *2013 European control conference* (pp. 511–517). Zurich: IEEE.

Cannon, M., Deshmukh, V., & Kouvaritakis, B. (2003). Nonlinear model predictive control with polytopic invariant sets. *Automatica*, *39*(8), 1487–1494.

Cannon, Mark, Kouvaritakis, Basil, & Deshmukh, Venkatesh (2004). Enlargement of polytopic terminal region in NMPC by interpolation and partial invariance. *Automatica*, *40*(2), 311–317.

Chen, Hong, & Allgöwer, Frank (1998). A quasi-infinite horizon nonlinear model predictive control scheme with guaranteed stability. *Automatica*, *34*(10), 1205–1217.

De Doná, J. A., Seron, M. M., Mayne, D. Q., & Goodwin, G. C. (2002). Enlarged terminal sets guaranteeing stability of receding horizon control. *Systems & Control Letters*, *47*(1), 57–63.

Formentin, Simone, & Lovera, Marco (2011). Flatness-based control of a quadrotor helicopter via feedforward linearization. In *IEEE conference on decision and control and European control conference* (pp. 6171–6176). Orlando, FL, USA: IEEE.

Gantmacher, Feliks Rouminovich (1960). The theory of matrices. volume one. ISBN: 8284-0131-4.

Gaßmann, Victor, & Althoff, Matthias (2022). Implementation of Ellipsoidal Operations in CORA 2022. *90*, In *EPiC Series in Computing* (pp. 1–17). EasyChair, [ISSN: 2398-7340] http://dx.doi.org/10.29007/p328.

Herceg, Martin, Kvasnica, Michal, Jones, Colin N., & Morari, Manfred (2013). Multi-parametric toolbox 3.0. In *2013 European control conference* (pp. 502–510). IEEE.

Karl, W. C., Verghese, G. C., & Willsky, A. S. (1994). Reconstructing Ellipsoids from Projections. *CVGIP: Graphical Models and Image Processing*, [ISSN: 1049-9652] *56*(2), 124–139. http://dx.doi.org/10.1006/cgip.1994.1012.

Limon, D., Alamo, T., & Camacho, E. F. (2005). Enlarging the domain of attraction of MPC controllers. *Automatica*, *41*(4), 629–635.

Lu, Hao, Liu, Cunjia, Guo, Lei, & Chen, Wen-Hua (2017). Constrained anti-disturbance control for a quadrotor based on differential flatness. *International Journal of Systems Science*, *48*(6), 1182–1193.

Magni, L., & Scattolini, R. (2004). Model predictive control of continuous-time nonlinear systems with piecewise constant control. *IEEE Transactions on Automatic Control*, *49*(6), 900–906.

Mayne, David Q., Rawlings, James B., Rao, Christopher V., & Scokaert, Pierre O. M. (2000). Constrained model predictive control: Stability and optimality. *Automatica*, *36*(6), 789–814.

Nascimento, Tiago P., & Saska, Martin (2019). Position and attitude control of multi-rotor aerial vehicles: A survey. *Annual Reviews in Control*, *48*, 129–146.

Nguyen, Ngoc Thinh (2019). *Reliable hierarchical control for multicopter systems, no. 2019GREAT061* (Ph.D. thesis), Université Grenoble Alpes.

Nguyen, Ngoc Thinh, Prodan, Ionela, & Lefèvre, Laurent (2020). Flat trajectory design and tracking with saturation guarantees: A nano-drone application. *International Journal of Control*, *93*(6), 1266–1279.

Nguyen, Ngoc Thinh, Prodan, Ionela, & Lefèvre, Laurent (2021). Stability guarantees for translational thrust-propelled vehicles dynamics through NMPC designs. *IEEE Transactions on Control Systems Technology*, *29*(1), 207–219.

Wächter, Andreas, & Biegler, Lorenz T. (2006). On the implementation of an interior-point filter line-search algorithm for large-scale nonlinear programming. *Mathematical Programming*, *106*(1), 25–57.

Huu Thien Nguyen received the Engineering degree in Mechatronics from the Ho Chi Minh City University of Technology, Ho Chi Minh City, Vietnam, in 2019. From February to July 2019, he was doing his master's thesis at the Laboratory of Conception and Integration of Systems (LCIS) of Grenoble INP, University Grenoble Alpes, Valence, France. Since 2020, he has been a Ph.D. Student in Applied Mathematics at the University of Porto, Porto, and a researcher at the R&D Unit SYSTEC (ISRP/FEUP) and since 2021, part of ARISE-LA, Portugal. His research interests are optimization and optimal control with applications in UAVs, including hybrid UAVs, fixed-wing UAVs, and multicopters.

Ngoc Thinh Nguyen received the Engineering degree in Mechatronics from the Ho Chi Minh City University of Technology, Ho Chi Minh City, Vietnam, in 2016, and the Ph.D. degree in Control Engineering from the Laboratory of Conception and Integration of Systems (LCIS), Valence, France, in 2019. He is currently a Post-Doctoral Researcher with the Institute for Robotics and Cognitive Systems, University of Lübeck, Germany. His research interests include system modeling, optimal control, and optimal trajectory generation for autonomous systems such as unmanned aerial vehicles (UAVs), mobile robots, and autonomous driving cars.

Ionela Prodan received the B.S. in Automation and Applied Informatics degree from the Univ. Politehnica of Bucharest, Romania in 2009 and her Ph.D. in Control Engineering from Supélec, Gif-sur-Yvette, France in 2012. She continued with a post-doctoral fellowship within the Chair on Systems Science and the Energetic Challenge - EDF, École Centrale Paris, France. Since 2014 she has been an Associate Professor at the Laboratory of Conception and Integration of Systems (LCIS) of Grenoble INP, Univ. Grenoble Alpes, Valence, France. She obtained her HDR (Habilitation to Conduct Research) in 2020. Her research interests are multi-disciplinary with a core expertise in control and applied mathematics. These encompass constrained optimization-based control (Model Predictive Control via distributed and decentralized approaches), mixed-integer programming, differential flatness, set-theoretic methods, and their application to motion planning for autonomous vehicles and energy management in building-scale DC microgrids. Dr. Prodan is a member of the IFAC Technical Committee 6.3. Power and Energy Systems and an Associate Editor for the EUCA European Control Conference.